Durante, M. G., Karamitros, D., Di Sarno, L., Sica, S., Taylor, C. A., Mylonakis, G., & Simonelli, A. L. (2015). Characterisation of shear wave velocity profiles of non-uniform bi-layer soil deposits: Analytical evaluation and experimental validation. Soil Dynamics and Earthquake Engineering, 75, 44-54. DOI: 10.1016/j.soildyn.2015.03.010

CHARACTERISATION OF SHEAR WAVE VELOCITY PROFILES OF NON-UNIFORM BI-LAYER SOIL DEPOSITS: ANALYTICAL EVALUATION AND EXPERIMENTAL VALIDATION

Maria Giovanna Durante[1], Dimitris Karamitros[2], Luigi Di Sarno[1], Stefania Sica[1], Colin A Taylor[2], George Mylonakis[2,3,4], Armando Lucio Simonelli[1]

[1] Department of Engineering, University of Sannio, Italy
[2] Department of Civil Engineering, University of Bristol, U.K.
[3] Department of Civil Engineering, University of Patras, Greece
[4] Department of Civil Engineering, University of California at Los Angeles

Corresponding author: Maria Giovanna Durante
telephone: +39 333 5451392
email address: mgdurante@unisannio.it

Abstract

A crucial aspect of physical geotechnical model tests (under both 1-g and n-g conditions) is the evaluation of the initial (low-strain) stiffness of the soil layers of the sample test deposit, especially in the case of coarse materials. While for uniform soil deposits this issue can be addressed in a straightforward manner, e.g. by determining the fundamental frequency through the transfer function of an applied white-noise excitation, the problem becomes cumbersome for multi-layered deposits. After reviewing a number of available theoretical solutions, this paper illustrates a simplified yet reliable analytical procedure for determining the shear wave velocity profile (V_s) in a single or bi-layer deposit, taking into account the inhomogeneity of the individual soil layers, under the hypothesis of vanishing shear modulus at ground surface. The fundamental natural frequency of the inhomogeneous bi-layer deposit is analysed using the Rayleigh quotient procedure. The associated shape function is evaluated by considering the equilibrium of the soil column under a pseudo-static lateral inertial excitation imposed at its base, accounting for both layering and inhomogeneity. A validation of the proposed method is provided by comparing numerical results obtained from both time- and frequency- domain analyses against experimental data on Leighton Buzzard sand, from a recently-completed research project conducted on the shaking table facility at BLADE Laboratory, University of Bristol (UK).

Keywords: Free field response; initial shear wave velocity; shaking table test; numerical simulation.

1. Introduction

Shear wave velocity at low strain is fundamentally related to material behaviour and associated constitutive modelling of granular soils. As a starting point for any subsequent response analysis, it is essential that low-strain behaviour is accurately characterised. The shear wave velocity of a single layer soil deposit in physical devices (e.g. a shaking table or a centrifuge) is generally estimated by correlating it to the fundamental natural frequency of the layer, to obtain a mean value corresponding to equivalent homogeneous conditions. Towata [1] demonstrated that taking into account the actual variation of shear modulus (and therefore shear wave velocity) with depth for single-layer deposits could allow an improved fitting of the experimental data. Such an approach was employed for different types of soil inhomogeneity and closed-form solutions were provided for the identification of the natural frequencies. In the same context, Dobry et al. [2], based on the previous works of Ambraseys [3] and Seed and Idriss [4], studied the dynamic response of an inhomogeneous soil with a variation in shear wave velocity of the form $V_s = cz^n$, i.e. a parabolic

function with zero value at ground surface, *n* being a positive inhomogeneity coefficient. In parallel, Ambraseys [3], Toki and Cherri [5], Schreyer [6] and Gazetas [7] examined heterogeneous soils with shear wave velocity starting from a non-zero value at ground surface, focusing on the effect of rate and type of inhomogeneity. Rovithis et al. [8] and Mylonakis et al. [9] explored the seismic response of an inhomogeneous soil layer over a homogeneous layer of higher stiffness, considering a parabolically varying shear wave propagation velocity. The special case of zero shear modulus at ground surface was also investigated. It was established that even in the case of moderately or strongly inhomogeneous soil, a pertinent equivalent shear wave velocity for all the deposit can be effectively used. In this context, Dobry et al. [10], following the early work of Madera [11], investigated approximate methods for estimating the fundamental natural period of a layered soil profile. Other dependable solutions have been presented by Sarma [12] and Vrettos [13], the latter considering bounded soil inhomogeneity of an exponential type.

Following in the same vein and using the Rayleigh quotient procedure, the authors developed a generalized closed-form solution for the prediction of the fundamental natural frequency of both single- and two-layer inhomogeneous deposits, taking into account a different inhomogeneity coefficient for each layer (Figure 1), under the hypothesis of zero shear modulus at the ground surface. Simplified closed-form solutions are also provided, for typical bi-layer deposits with different combinations of inhomogeneity coefficients. The fundamental frequency is expressed as a function of the ratio of the thicknesses of the two layers, their densities and their shear wave velocities at the bottom of the deposit, as well as the shear wave velocity of the top layer. Given that the layer thicknesses, the soil densities, as well as the soil types, and thus the corresponding inhomogeneity coefficients are easy to establish experimentally, the proposed relations can be utilized to either estimate the fundamental frequency of the bi-layered soil deposit as a function of the ratio of shear wave velocities, or vice versa. In both cases, it is required to know the shear wave velocity of the top layer, which is easy to determine through the fundamental frequency of the transfer function between the soil surface and the layers interface for any applied signal.

In the above derivation, the shape function of the deposit is not assumed to be sinusoidal, as done by previous researchers (e.g. [9]), but it is obtained from the lateral equilibrium of a soil column featuring the same layering and inhomogeneity characteristics. The proposed closed-form solution is validated through comparisons of numerical analyses performed with the analytically predicted shear wave velocity profiles, against experimental results from high-quality shaking table tests carried out within the framework of the SERIES project *PILESI* [14]. In this project, the free field response of a bi-layer Leighton Buzzard sand deposit subject to dynamic excitations has been

thoroughly investigated on the shaking table at BLADE laboratory of University of Bristol (UK), and relevant numerical simulations were performed.

2. Analytical investigation

The analytical investigation presented herein focuses upon two different cases: a single inhomogeneous layer (Figure 1a) and an inhomogeneous two-layer deposit (Figure 1b), over a rigid base. In both cases, mass density (ρ) is considered constant for each layer, while the shear modulus increases with depth according to the expression:

$$G(z)=G_B\left(\frac{z}{H}\right)^b \tag{1}$$

where G_B is the shear modulus at the bottom of the deposit, b is a dimensionless coefficient related to soil inhomogeneity and z is depth measured from ground surface.

The equations governing one-dimensional shear wave propagation under harmonic oscillations in an inhomogeneous soil column can be written as:

$$\frac{d}{dz}\left[G(z)\frac{du}{dz}\right]+\rho\omega^2 u=0 \tag{2}$$

As demonstrated by Mylonakis et al. [9], the natural frequencies of the system may be derived from the familiar Rayleigh quotient:

$$\omega^2=\frac{\int_0^H G(z)\left(\frac{du(z)}{dz}\right)^2 dz}{\int_0^H \rho[u(z)]^2 dz} \tag{3}$$

Substituting $u(z)=u_0\psi(z)$, the above equation can be written as:

$$\omega^2=\frac{\int_0^H G(z)\left(\frac{d\psi(z)}{dz}\right)^2 dz}{\int_0^H \rho[\psi(z)]^2 dz} \tag{4}$$

where $\psi(z)$ is a dimensionless shape function representing, approximately, the mode shape corresponding to the fundamental natural frequency of the inhomogeneous soil deposit. The shape function is obtained using a simple procedure [15] as depicted in Figure 2. More specifically, the mode of deformation is determined as the lateral movement of the soil column, modelled as a shear beam, under a distributed horizontal load, equal to its self-weight, considering the origin of displacement axis at the top of the soil column. This allows taking into account the variations of both unit weight and shear modulus with depth.

In this context:

$$u(z)=\int_0^z \gamma(z)dz=\int_0^z \frac{\rho(z)gz}{G(z)}dz \tag{5}$$

where $\gamma(z)$ is the engineering shear strain.

The shape function employed in the Rayleigh quotient is unitary at ground surface and zero at the base, to satisfy the essential boundary conditions of the problem. Therefore,

$$\psi(z)=1-\frac{\int_0^z \frac{\rho(z)gz}{G(z)}dz}{\int_0^H \frac{\rho(z)gz}{G(z)}dz} \tag{6}$$

Specific forms of the above shape function can be written by considering the cases shown in Figure 1a,b, using Equation 1.

For instance, for a single layer having constant density, it becomes:

$$\psi(\bar{z})=1-\bar{z}^{2-b} \tag{7}$$

where $\bar{z}=z/H$ is the dimensionless depth.

Figure 3 compares the proposed shape function for a homogeneous single layer (obtained by setting *b=0* in equation 7) against the theoretical shape function which is sinusoidal. It may be observed that this simplified procedure approximates the exact analytical solution with reasonable accuracy and may therefore be readily employed to handle the more complicated cases examined herein.

For the two-layer inhomogeneous deposit in Figure 1b, the shape function is obtained as follows:

$$\psi(z)=\frac{1}{D}\begin{cases}\left[\frac{\bar{h}_1^{2-b_1}-\bar{z}^{2-b_1}}{2-b_1}+\alpha\frac{1-\bar{h}_1^{2-b_2}}{2-b_2}\right] & 0\le\bar{z}\le\bar{h}_1\\ \left[\frac{\alpha}{2-b_2}\left(1-\bar{z}^{2-b_2}\right)\right] & \bar{h}_1\le\bar{z}\le1\end{cases} \tag{8}$$

where $\overline{h_1}=h_1/H$ is the dimensionless thickness of the upper layer, and:

$$D=\frac{\bar{h}_1^{2-b_1}}{2-b_1}+\alpha\frac{1-\bar{h}_1^{2-b_2}}{2-b_2} \tag{9}$$

$$\alpha=\left(\frac{V_{s1,B}}{V_{s2,B}}\right)^2 \tag{10}$$

$$V_{s1,B}=\sqrt{\frac{G_{1,B}}{\rho_1}} \qquad V_{s2,B}=\sqrt{\frac{G_{2,B}}{\rho_2}} \tag{11a,b}$$

Figure 4 compares the sinusoidal shape function against the proposed one (the latter obtained assuming *b₁=b₂=0.5* in equation 8) for an inhomogeneous two-layer deposit with $\overline{h_1}=0.5$ and $a=0.5$. Evidently, the shape function for multilayered deposits cannot be well approximated by a sinusoidal function. This indicates that employing the procedure at hand is important in calculating the natural frequency of the system.

2.1. Single inhomogeneous layer

Referring to the single inhomogeneous soil layer in Figure 1a, equation 4 becomes:

$$\omega^2=\frac{G_B \int_0^H \left(\frac{z}{H}\right)^b \left(\frac{d\psi(z)}{dz}\right)^2 dz}{\rho \int_0^H [\psi(z)]^2 dz} \tag{12}$$

Substituting the shape function in Eq 12, one obtains:

$$\omega^2=\frac{(2-b)^2(5-2b)}{2\left(b^2-4b+4\right)} \frac{{V_{s,B}}^2}{H^2} \tag{13}$$

Three simple cases can be obtained from this solution by considering typical values of *b*:

- *b≈0*, corresponding to a homogeneous layer, typical of over-consolidated clay:

$${\omega^2}_{b=0}=\frac{5}{2}\frac{{V_{s,B}}^2}{H^2}\cong 2.5\frac{{V_{s,B}}^2}{H^2} \tag{14}$$

In this case, the corresponding shear wave velocity at the bottom of the layer is given by:

$$V_{s,B}\cong 3.97fH \tag{15}$$

f being the natural frequency (in units of 1/Time) of the layer.

Note that above the solution is very close to the exact one ($V_s=4fH$), the difference being due to the slight deviation of the generalized parabolic function in Eq. 7 from a perfect sinusoid.

- *b≈0.5*, typical of a sand deposit:

$${\omega^2}_{b=0.5}\cong 2\frac{{V_{s,B}}^2}{H^2} \tag{16}$$

In this case, the corresponding shear wave velocity at the bottom of the layer is given by:

$$V_{s,B}\cong 4.44fH \tag{17}$$

This solution can be compared against the results of Towhata [1]. Under the same assumptions, the shear wave velocity at the bottom of the layer is evaluated as:

$$V_{s,B,\,T}=4.49fH \tag{18}$$

which is in meaningful agreement with equation 17.

- *b≈1*, typical of a normally-consolidated clay deposit:

$${\omega^2}_{b=1}\cong\frac{3}{2}\frac{{V_{s,B}}^2}{H^2}\cong 1.5\frac{{V_{s,B}}^2}{H^2} \tag{19}$$

In this case, the corresponding shear wave velocity at the bottom of the layer is given by:

$$V_{s,B}\cong 5.13fH \tag{20}$$

According to Towata [1], the shear wave velocity at the bottom of the layer is evaluated as:

$$V_{s,B,\,T}=5.22fH \tag{21}$$

which is again in meaningful agreement with the proposed solution.

2.2. Two-layer inhomogeneous deposit

Referring to Figure 1b and the shape function in Eq. 8, the solution to Eq. 4 becomes:

$$\omega^2=\frac{G_{1,B}\int_0^{h_1}\left(\frac{z}{H}\right)^{b_1}\left(\frac{d\psi(z)}{dz}\right)^2 dz+G_{2,B}\int_{h_1}^{H}\left(\frac{z}{H}\right)^{b_2}\left(\frac{d\psi(z)}{dz}\right)^2 dz}{\rho_1\int_0^{h_1}[\psi(z)]^2dz+\rho_2\int_{h_1}^{H}[\psi(z)]^2dz} \tag{22}$$

Evaluating the integrals, equation 22 can be written as:

$$\omega^2=\frac{A_1+\alpha\,\alpha_1 A_2}{A_3+\alpha^2\alpha_1 A_4}\frac{V_{s1,B}^2}{H^2} \tag{23}$$

where $\alpha_1=\rho_2/\rho_1$ and

$$A_1=\frac{\bar{h}_1^{3-b_1}}{3-b_1} \tag{24}$$

$$A_2=\frac{1-\bar{h}_1^{3-b_2}}{3-b_2} \tag{25}$$

$$A_3=\frac{\bar{h}_1^{5-2b_1}}{(2-b_1)^2(5-2b_1)}+C^2\bar{h}_1-2\frac{C\bar{h}_1^{3-b_1}}{(2-b_1)(3-b_1)} \tag{26}$$

$$A_4=\frac{1}{(2-b_2)^2}\left(1-\bar{h}_1+\frac{1-\bar{h}_1^{5-2b_2}}{5-2b_2}-2\frac{1-\bar{h}_1^{3-b_2}}{3-b_2}\right) \tag{27}$$

$$C=\frac{\bar{h}_1^{2-b_1}}{2-b_1}+\alpha\frac{1-\bar{h}_1^{2-b_2}}{2-b_2} \tag{28}$$

Although the above solution is simple to implement, a graphical form of the results is also provided for routine use (Figure 5), without the need for a spreadsheet or a pocket calculator. The format utilized for the graphical representation is the same as the one adopted by Madera [11], where the ratio of the deposit eigenvalue T over the top layer eigenvalue T_1 is provided as a function of the layer thickness ratio h_1/h_2 and the stiffness ratio $(V_{s1}h_2)/(V_{s2}h_1)$. Nine cases are examined for various combinations of over-consolidated clay (b=0), sand (b=0.5) and normally-consolidated clay (b=1) layers. Note that the first graph of Figure 5 corresponds to the same case examined by Madera and that a very good agreement is observed. The corresponding analytical expressions for each case are as follows:

- Case 1: over-consolidated clay over over-consolidated clay *($b_1=b_2=0$)*, $\alpha_1=1$

$$\omega^2=\frac{5\bar{h}_1^3+5\alpha\left(1-\bar{h}_1^3\right)}{\bar{h}_1^5(3\alpha^2-5\alpha+2)+5\alpha\bar{h}_1^3(1-\alpha)+2\alpha^2}\frac{V_{s1,B}^2}{H^2} \tag{29}$$

- Case 2: sand over sand *($b_1=b_2=0.5$)*, $\alpha_1=1$

$$\omega^2=\frac{9\bar{h}_1^{2.5}+9\alpha\left(1-\bar{h}_1^{2.5}\right)}{\bar{h}_1^{4}(7.5\alpha^2-12\alpha+4.5)+12\alpha\bar{h}_1^{2.5}(1-\alpha)+4.5\alpha^2}\frac{V_{s1,B}^2}{H^2} \tag{30}$$

- Case 3: normally-consolidated clay over normally-consolidated clay *(b_1=b_2=1)*, $\alpha_1 = 1$

$$\omega^2=\frac{1.5\bar{h}_1^{2}+1.5\alpha\left(1-\bar{h}_1^{2}\right)}{\bar{h}_1^{3}(2\alpha^2-3\alpha+1)-3\alpha\bar{h}_1^{2}(\alpha-1)+\alpha^2}\frac{V_{s1,B}^2}{H^2} \tag{31}$$

- Case 4: over-consolidated clay over sand *(b_1=0 b_2=0.5)*, $\alpha_1 = 1$

$$\omega^2=\frac{7.5\bar{h}_1^{3}+9\alpha\left(1-\bar{h}_1^{2.5}\right)}{3\bar{h}_1^{5}-10\alpha\bar{h}_1^{4.5}+7.5\alpha^2\bar{h}_1^{4}+10\alpha\bar{h}_1^{3}-12\alpha^2\bar{h}_1^{2.5}+4.5\alpha^2}\frac{V_{s1,B}^2}{H^2} \tag{32}$$

- Case 5: over-consolidated clay over normally-consolidated clay *(b_1=0 b_2=1)*, $\alpha_1 = 1$

$$\omega^2=\frac{2\bar{h}_1^{3}+3\alpha\left(1-\bar{h}_1^{2}\right)}{0.8\bar{h}_1^{5}-4\alpha\bar{h}_1^{4}+4\alpha\bar{h}_1^{3}(\alpha+1)-6\alpha^2\bar{h}_1^{2}+2\alpha^2}\frac{V_{s1,B}^2}{H^2} \tag{33}$$

- Case 6: sand over over-consolidated clay *(b_1=0.5 b_2=0)*, $\alpha_1 = 1$

$$\omega^2=\frac{3\bar{h}_1^{2.5}+2.5\alpha\left(1-\bar{h}_1^{3}\right)}{1.5\alpha^2\bar{h}_1^{5}-3\alpha\bar{h}_1^{4.5}+1.5\bar{h}_1^{4}-2.5\alpha^2\bar{h}_1^{3}+3\alpha\bar{h}_1^{2.5}+\alpha^2}\frac{V_{s1,B}^2}{H^2} \tag{34}$$

- Case 7: sand over normally-consolidated clay *(b_1=0.5 b_2=1)*, $\alpha_1 = 1$

$$\omega^2=\frac{1.2\bar{h}_1^{2.5}+1.5\alpha\left(1-\bar{h}_1^{2}\right)}{0.6\bar{h}_1^{4}-2.4\alpha\bar{h}_1^{3.5}+2\alpha^2\bar{h}_1^{3}+2.4\alpha\bar{h}_1^{2.5}-3\alpha^2\bar{h}_1^{2}+\alpha^2}\frac{V_{s1,B}^2}{H^2} \tag{35}$$

- Case 8: normally-consolidated clay over over-consolidated clay *(b_1=1 b_2=0)*, $\alpha_1 = 1$

$$\omega^2=\frac{3\bar{h}_1^{2}+2\alpha\left(1-\bar{h}_1^{3}\right)}{1.2\alpha^2\bar{h}_1^{5}-3\alpha\bar{h}_1^{4}-2\bar{h}_1^{3}(\alpha^2-1)+3\alpha\bar{h}_1^{2}+0.8\alpha^2}\frac{V_{s1,B}^2}{H^2} \tag{36}$$

- Case 9: normally-consolidated clay over sand *(b_1=1 b_2=0.5)*, $\alpha_1 = 1$

$$\omega^2=\frac{3.75\bar{h}_1^{2}+3\alpha\left(1-\bar{h}_1^{2.5}\right)}{2.5\alpha^2\bar{h}_1^{4}-5\alpha\bar{h}_1^{3.5}+2.5\bar{h}_1^{3}-4\alpha^2\bar{h}_1^{2.5}+5\alpha\bar{h}_1^{2}+1.5\alpha^2}\frac{V_{s1,B}^2}{H^2} \tag{37}$$

3. Validation

To verify the accuracy of the proposed solution, the results from a series of numerical analyses in both the time and frequency domain, performed using the analytically-predicted shear wave velocities of a bi-layer soil deposit, are compared against corresponding experimental data from

shaking table tests. More specifically, the experimental data set relies on comprehensive high-quality shaking table tests carried out within the framework of the Seismic Engineering Research Infrastructures for European Synergies (SERIES), as a part of PILESI project [14]. The tests were performed at the Bristol Laboratory for Advanced Dynamics Engineering (BLADE), so the 6-degree-of-freedom earthquake simulator and the equivalent shear beam (ESB) laminar container of BLADE were utilized to this end.

In the PILESI project, the tests were focusing on pile behaviour, aiming to investigate various aspects of Seismic Soil-Pile-Structure-Interaction (SSPSI), such as the natural frequency of the systems in both horizontal and vertical directions, the natural frequency and damping of the embedded piles, the horizontal and vertical soil-pile kinematic interaction and the foundation-structure interaction. The scaled model, standing on the *1-g* shaking table, was formed by a group of five piles embedded in a bi-layer soil deposit (Figure 6). Different pile group configurations were considered, with and without pile caps and superstructures, subjected to both lateral and vertical earthquake shaking. The loading conditions include different excitations such as white noise, sine dwells and earthquake ground motions. Nevertheless, this paper only focuses on the free field response of the bi-layer deposit, looking at the response of accelerometers located in a vertical array, at sufficient distance from both the piles and the boundaries of the equivalent shear beam container, to avoid interaction effects on soil response. The response of the whole system has been analysed in other studies [14, 16-19].

The bi-layer deposit in the examined configuration consisted of a 0.44m thick layer of dense sand, overlaid by a0.36m thick layer of loose sand. To achieve a proper stiffness contrast between the top and bottom layers, two different types of dry sands ($S_r = 0$) were utilised: the bottom layer was a mix of Leighton Buzzard (LB) Sand Fractions B and E (*85%* and *15%* respectively), pluviated through a 12mm diameter nozzle to achieve a high mass density ($\rho_2 = 1780\ kg/m^3$); the top layer was made of LB Fraction E Sand, deposited through a 40mm diameter nozzle to achieve a lower mass density ($\rho_1 = 1390\ kg/m^3$). Leighton Buzzard sand has been extensively used in experimental research activities carried out at BLADE and other laboratories; hence measured density and stiffness values are available [20-27]. Table 1 lists the index properties of LB sand from the above cited literature. The particular properties of the two soil layers constituting the sample models of the PILESI experimental campaign are reported in Table 2.

As previously described, the experimental campaign consisted of more than *300* tests. In this paper, only a small set of the available data has been considered, corresponding to the White Noise (WN) input motion at low amplitude and some sine dwell tests. The employed WN excitation is a random noise signal of bandwidth *0-100* Hz and maximum acceleration of *0.019g*. This form of excitation is

typically adopted in centrifuge or shaking table tests to estimate the natural frequency of the system at different strain levels. As far as the sine dwell tests employed herein are concerned, they involve sinusoidal motions with a constant frequency of 30Hz and amplitudes varying from 0.003 to 0.06g, as well as motions with a constant amplitude of 0.04g and frequencies varying from 15 to 30Hz.

A preliminary evaluation of the initial stiffness G_0 of the two soil layers has been performed by the Hardin & Drnevich empirical equation [28]:

$$G_0=\frac{3230\cdot(2.973-e)^2}{1+e}\sqrt{\sigma'_m} \tag{38}$$

where σ'_m and e are the mean effective stress and the void ratio, respectively. For the evaluation of σ'_m in the soil inside the shear stack, the k_0 coefficients proposed by Stroud [21] were adopted, i.e. *0.445* and *0.46* for the dense and loose Leighton Buzzard sand, respectively. As expected, these shear wave velocities increase with the fourth root of depth and correspond to values of $V_{s1,B}$= *79.5m/s* and $V_{s2,B}$= *132.8m/s* at the bedrock.

In order to employ the proposed methodology for a more accurate estimation of the shear wave velocity profile, the fundamental frequencies of the the upper layer (f_1) and of the overall deposit (f_{tot}) were obtained, by analyzing the accelerograms recorded during the White Noise test, along a monitored free-field vertical array inside the deposit. More specifically, the Fourier spectra of the acceleration recordings at the model's base, at the interface of the two layers and at ground surface were initially computed. Then, the transfer functions from the bedrock to the soil surface and from the two layers' interface to the soil surface were calculated (Figure 7), by dividing the corresponding spectra. Finally, the fundamental frequencies were determined, by fitting, in terms of natural frequencies f_{nat} and damping ratio D, the following theoretical expression for a visco-elastic homogeneous layer over a rigid base:

$$A(f)=\frac{1}{\sqrt{\cos^2 F+(FD)^2}} \tag{39}$$

where F is the frequency factor, given by:

$$F(f)=\frac{\omega H}{V_s}=\frac{\pi f}{2f_{nat}} \tag{40}$$

The computed frequencies, namely f_1=*38.9Hz* and f_{tot}=*26.9Hz*, allow the evaluation of the shear wave velocity profile of the model, by means of the proposed method, with $b_1=b_2=0.5$, first using Eq 17 for the evaluation of shear wave velocity $V_{s1,B}$ for the top layer, and then Eq 23 for the evaluation of $V_{s2,B}$ for the underlying one. The values obtained using this procedure are $V_{s1,B}$=*72.8m/s* and $V_{s2,B}$=*93.9m/s*, while the corresponding shear wave velocity profile is shown in Figure 8a. Nevertheless, it was found that the corresponding shear moduli are not actually the initial ones. This is because, in spite of the low excitation amplitude employed in the White Noise test, the

shear strains induced in the soil deposit were not negligible. In fact, if the aforementioned shear wave velocity profiles were considered in a ground response analyses with EERA [29], shear strains between $2 \cdot 10^{-5}$ and $4 \cdot 10^{-5}$ would be predicted for the White Noise test, corresponding to a stiffness degradation of 10-20%. The resulting degraded shear wave velocities are compared with the initially predicted ones in Figure 8a.

In order to account for this effect, the analytically computed shear wave velocities were increased by 12% for the top layer and 7% for the bottom one, to $V_{s1,B}=81.7m/s$ and $V_{s2,B}=100.6m/s$, with the resulting shear wave velocity profile being shown in Figure 8b. Repeating the ground response analyses for the White Noise Test with the updated profile, the degraded shear wave velocity profile may be similarly obtained. As it may be observed in Figure 8b, these degraded shear wave velocities are in good agreement with the ones initially obtained with the analytical methodology. Furthermore, the numerically obtained transfer functions for both the whole system and the top layer are plotted in Figure 7, indicating a meaningful agreement with the experimentally computed ones. In fact, Table 3 highlights that in terms of resonance frequency, the difference between numerical analyses and experimental results is not larger than 2.3%.

The finally adopted shear wave velocity profile is compared to the one determined by the Hardin & Drnevich relationship in Figure 9. These are also compared to the uniform shear wave velocities that would have been computed according to Madera's method (or, equivalently, the proposed method with $b_1=b_2=0$), namely $V_{s1}= 52.9\ m/s$ and $V_{s2}=89.2\ m/s$. It should be noted that the same experimental data have been analysed by Chidichimo et al [19], whose estimations are in good agreement with the Madera results, namely $V_{s1}=52m/s$ and $V_{s2}=87m/s$.

To assess the validity of the above shear wave velocity profiles, two different types of numerical analyses were carried out, namely in the frequency and the time domain. In both cases, the Vucetic and Dobry curves (1991) for zero plasticity index [30] were chosen for the variation of shear modulus and damping ratio with cyclic shear strain amplitude. The analyses in the frequency domain were performed with the EERA code, considering an equivalent-linear soil behaviour, with the aforementioned degradation curves $G(\gamma)$ and $D(\gamma)$.

The analyses in the time domain were carried out with the explicit finite difference code FLAC [31]. In order to simulate the hysteretic soil behaviour, a multiaxial formulation of the Ramberg-Osgood stress-strain relationship was employed, implemented into FLAC as a user-defined constitutive model. According to this formulation, the tangent shear modulus is computed as follows:

$$G_t=\frac{G_0}{T} \tag{41}$$

where:

$$T=\begin{cases} 1+2\left(\frac{1}{\alpha_1}-1\right)\frac{|X|}{\eta_1} & \text{for initial shearing} \\ 1+2\left(\frac{1}{\alpha_1}-1\right)\frac{|X^{LR}|}{2\eta_1} & \text{after the first load reversal} \end{cases} \quad (42)$$

with:

X scalar measure of the deviatoric stress ratio (X^{LR} is the value at last load reversal), evaluated as:

$$X=\sqrt{\frac{1}{2}\left(r_{ij}-r_{ij}^{LR}\right)\left(r_{ij}-r_{ij}^{LR}\right)} \quad (43)$$

r_{ij} deviatoric stress ratio (r_{ij}^{LR} is the value at last load reversal), defined as the ratio of the deviatoric stress tensor $s_{ij}=\sigma'_{ij}-\sigma'_m\cdot\delta_{ij}$ over the mean effective stress $\sigma'_m=\sigma'_{kk}/3$;

η_1 model parameter defined as:

$$\eta_1=\alpha_1\left(\frac{G_{max}^{LR}}{\sigma^{LR}}\right)\gamma_1 \quad (44)$$

G^{LR}_{max} the maximum shear modulus at last load reversal;

σ^{LR} the isotropic stress at last load reversal;

α_1 and γ_1 model parameters.

The calibration of the two model parameters requires fitting of the Ramberg-Osgood predicted soil behaviour against the experimental *G(γ)* and *D(γ)* curves; in this work $\alpha_1=0.064$ and $\gamma_1=0.00016$ are used, which correspond to the best fitting of Vucetic and Dobry curves (1991) for zero plasticity index (Figure 10). To compensate for the low damping response of the model at small strain levels, an additional Rayleigh damping of 5% is added.

Figure 11 shows the comparison between the experimental data and the numerical results obtained with both methods, for a sinusoidal input motion characterized by a frequency of *30* Hz and an amplitude of *0.003g*. Firstly, it should be highlighted that the results produced by the analyses in both the frequency and the time domains are almost identical. Furthermore, the agreement, both in terms of maximum accelerations and shape functions, is very satisfactory, with the exception of the slightly lower experimental accelerations in the top layer. This discrepancy, however, is attributed to an over-damping effect induced by the shear beam (ESB) laminar container [19, 32]. It should be stressed out that this effect is only observed for small input excitation amplitudes, where the soil behaviour is almost linear elastic and the associated hysteretic damping is small. Indeed, the acceleration diagrams obtained for higher amplitude (0.02g and 0.06g) input motions (Figure 12) show a good agreement along the whole soil profile, as, in these cases, it is the soil non-linear

behaviour that governs the system's performance. This observation demonstrates that the overall accuracy of the shear wave velocity profile obtained with the proposed methodology is satisfactory.

Furthermore, the numerical analyses have been repeated, in all the above cases, considering homogeneous soil profiles. The corresponding results are added to Figures 11 and 12, for the sake of comparison. This way, it is observed that considering an homogeneous soil profile, it is not possible to capture the soil response close to the interface between the two layers. This is due to the associated large contrast in the shear modulus, which is not the case for the physical model.

A further comparison between experimental and numerical analyses is performed for two input motions characterized by the same amplitude (*0.04g*) and different frequencies (*15* and *30* Hz): the results are illustrated in Figure 13 and they demonstrate the very good agreement between measured and computed maximum accelerations for both the exciting frequencies, highlighting the importance of taking into account the effect of soil inhomogeneity.

4. Conclusions

Closed-form solutions for the initial stiffness of single- and two-layer inhomogeneous deposits, with zero shear modulus at ground surface, are developed by employing the Rayleigh quotient procedure. The proposed relations are validated against high-quality shaking table tests, which indicate a meaningful agreement for all combinations of frequencies and input accelerations considered.

The outcomes of the numerical simulations are:

- The adoption of a homogeneous profile leads to an underestimation of interface acceleration, even though it provides reasonable values of surface acceleration;
- The inhomogeneous profiles for bi-layer soil deposits predict reasonably well both the acceleration at the surface and that at the interface between the two layers.
- Assessment of damping in the data at hand is not straightforward due to the contribution of the laminar box.

From a practical viewpoint, the method proposed in the present work may be easily employed for analysing experimental results obtained from shaking table or centrifuge tests, provided that the fundamental natural frequency of the deposit is properly evaluated by experimental means.

Acknowledgments

The research leading to these results has received funding from the European Union Seventh Framework Programme (FP7/2007-2013) for access to the Bristol Laboratory for Advanced Dynamics Engineering (BLADE), University of Bristol, UK under grant agreement n° 227887

[SERIES]. The financial support provided by the project ReLUIS (Task MT2) funded by the Italian Civil Protection is also appreciated.

The authors would like to acknowledge all the contributors to the SERIES project, namely: Prof. Subhamoy Bhattacharya from University of Surrey, Dr. Matthew Dietz and Dr. Luiza Dihoru from University of Bristol, Prof. Gianni Dente, Dr. Roberto Cairo and Dr. Andrea Chidichimo from University of Calabria, Prof. Arezou Modaressi and Dr. Luìs A. Todo Bom from Ecole Centrale Paris, Prof. Amir M. Kaynia from Norwegian University of Science and Technology and Dr. George Anoyatis from University of Patras.

References

[1] Towhata I. Seismic wave propagation in elastic soil with continuous variation of shear modulus in the vertical direction. Soils Found 1996; 36(1): 61-72

[2] Dobry R, Whitman R and Roesset JM. Soil properties and the one dimensional theory of earthquake amplification. Research Report 1971, R71-18, M.I.T.

[3] Ambraseys NN. A note on the response of an elastic overburden of varying rigidity to an arbitrary ground motion. Bull Seism Soc Am 1959; 49(3):211-220

[4] Seed HB, Idriss IM. The influence of ground conditions on ground motions during earthquakes. J Soil Mech Found 1969; Div 94: 93-137

[5] Toki K, Cherry S. Inference of subsurface accelerations and strain from accelerograms recorded at ground surface. Proceedings of the 4th European Symposium on Earthquake Engineering. London, 1972

[6] Schreyer H. One-dimensional elastic waves in inhomogeneous media. J Eng Mech Div ASCEE 1977; 103(5): 979-990

[7] Gazetas G. Vibrational characteristics of soil deposits with variable wave velocity. International J Num Anal Meth Geomech 1982; 6:1-20

[8] Rovithis E, Parashakis Ch, Mylonakis G. 1D harmonic response of layered inhomogeneous soil: analytical investigation. Soil Dyn Earth Eng 2011; 31(7): 879 - 890

[9] Mylonakis GE, Rovithis E, Parashakis H. 1D harmonic response of layered inhomogeneous soil: Exact and approximate analytical solutions. Computational Methods in Earthquake Engineering 2013; Computational methods in Applied Sciences Volume 30: 1-32

[10] Dobry R, Oweis I, Urzua A. Simplified procedures for estimating the fundamental period of a soil profile. Bull Seism Soc Am 1976; 66(4): 1293-1321

[11] Madera GA. Fundamental period and amplification of peak acceleration in layered systems. Research Report 1970, R70-37, M.I.T.

[12] Sarma, S.K. Analytical solution to the seismic response of visco-elastic soil layers, Geotechnique, 44 (2), 1994, pp. 265-275.

[13] Vrettos, C. Dynamic response of soil deposits to vertical SH waves for different rigidity depth-gradients. Soil Dynamics and Earthquake Engineering, 47, 2013, pp. 41-50.

[14] Simonelli AL, Di Sarno L, Durante MG, Sica S, Bhattacharya S, Dietz M, Dihoru L, Taylor CA, Cairo R, Chidichimo A, Dente G, Modaressi A, TodoBom LA, Kaynia AM, Anoyatis G, Mylonakis G. Chapter 27: Experimental Assessment of Seismic Pile-Soil Interaction. Seismic Evaluation and Rehabilitation of Structures, Geotechnical, Geological and Earthquake Engineering 2014; Volume 26:455-475

[15] Clough, R.W., Penzien J. Dynamics of Structures 1993. New York: McGraw-Hill. 2nd Edition

[16] Simonelli A.L., Di Sarno L., Durante M.G., Sica S., Bhattacharya S., Dietz M., Dihoru L., Taylor C.A., Cairo R., Chidichimo A., Dente G., Anoyatis G., Mylonakis G., Modaressi A., TodoBom L.A. and Kaynia A.M. Performance of soil-pile-structure systems under seismic waves. Proceeding of the II Int. Conf. on Performance-Based Design in Earthquake Geotechnical Engineering, Taormina 2012, I

[17] Simonelli A.L., Di Sarno L., Durante M.G., Sica S., Bhattacharya S., Dietz M., Dihoru L., Taylor C.A., Cairo R., Chidichimo A., Dente G., Anoyatis G., Mylonakis G., Modaressi A., TodoBom L.A. and Kaynia A.M. Experimental investigation of soil-pile-structure seismic interaction. Proceeding of the 15th World Conference on Earthquake Engineering, Lisbon 2012

[18] Durante M.G., Di Sarno L., Sica S., Mylonakis G., Taylor C., Simonelli A.L. Seismic Pile-Soil Interaction: Experimental results vs. numerical simulations. Proceeding of the 4th Intern. Conf. on Computational Methods in Structural Dynamics and Earthquake Engineering. M. Papadrakakis, V. Papadopoulos, V. Plevris (eds.), Kos Island, Greece, 2013

[19] Chidichimo A, Cairo R, Dente G, Taylor C, Mylonakis G. 1-g experimental investigation of bi-layer soil response and kinematic pile bending, Soil Dynamics and Earthquake Engineering 2014; in press.

[20] Seed B. H., Idriss I. M. Soil moduli and damping factors for dynamic response analyses. Earthquake engineering research center, report no. EERC 70-10, December 1970

[21] Stroud M A. The behaviour of sand at low stress levels in the simple shear apparatus. PhD thesis, University of Cambridge, UK; 1971

[22] Tan FSC. Centrifuge and theoretical modelling of conical footings on sand. PhD Thesis, University of Cambridge, UK; 1990

[23] Cavallaro A, Maugeri M, Mazzarella R. Static and dynamic properties of Leighton Buzzard sand from laboratory tests. 4th International Conference on Recent Advances in Geotechnical Earthquake Engineering and Soil Dynamics 2001, San Diego, CA, Paper 1.13

[24] Lings ML, Dietz MS. An improved direct shear apparatus for sand. Geotechnique 2004; 54: 4, 245–256

[25] Moccia F. Seismic soil pile interaction: experimental evidence. PhD Thesis, Universita' degli Studi di Napoli Federico II, Napoli; 2009

[26] Visone C, Santucci de Magistris F. Mechanical behaviour of the Leighton Buzzard Sand 100/170 under monotonic, cyclic and dynamic loading conditions. Proceeding of the XIII conference: L'ingegneria Sismica in Italia, ANIDIS, Bologna, Italy, 2009

[27] Bui M, Influence of some particle characteristics on the small strain response of granular materials. PhD Thesis, University of Southampton, 2009

[28] Hardin BO, Drnevich VP. Shear modulus and damping in soils: Design equations and curves. Journal of Soil Mechanics and Foundations Division, ASCE 1972. 98(7): 667-692

[29] Bardet JP, Ichii K, Lin CH. EERA a Computer Program for Equivalent-linear Earthquake site Response Analyses of Layered Soil Deposits. Univ of Southern California, Dep of Civil Eng.; 2000

[30] Vucetic M, Dobry R. Effect of soil plasticity on cyclic response. Journal of Geotechnical Engineering, ASCE 1991; Vol. 117 (1), pp. 89-107

[31] Itasca. FLAC – Fast Lagrangian Analysis of Continua – Version 5.0. Itasca Consulting Group, Inc., Minneapolis, USA; 2005

[32] Dietz M., Muir Wood D., Shaking table evaluation of dynamic soil properties. Proceeding of the 4th International Conference on Earthquake Geotechnical Engineering, Thessalonikki, Greece; 2007

Tables

Table 1. Leighton Buzzard sand: index properties from the referred literature

Materials	Type	γ_s [kN/m^3]	e_{min}	e_{max}	D_{10}	D_{50}	References
LB fraction E	Sand BS 881-131	25.96	0.613	1.014	0.095	0.14	Tan [20]
LB fraction B	Sand BS 881-132	25.96	0.486	0.78	0.63	0.76	Ling & Dietz [22]
LB fraction B+E		25.96	0.289	0.614			Moccia [23]

Table 2. Leighton Buzzard sand: properties of the soil layers in PILESI tests

	γ_s [kN/m^3]	e
Upper layer (LB E)	13.63	0.90
Bottom layer (LB B+E)	17.45	0.49

Table 3. Fundamental frequency of the system (f_{tot}) and the top layer (f_1) for white noise input (a_{max}=0.019*g*): experimental and numerical results

	Experimental	Numerical (frequency domain analysis)	Variation [%]
f_{tot} [Hz]	26.9	26.3	2.23
f_1 [Hz]	38.9	38.4	1.29

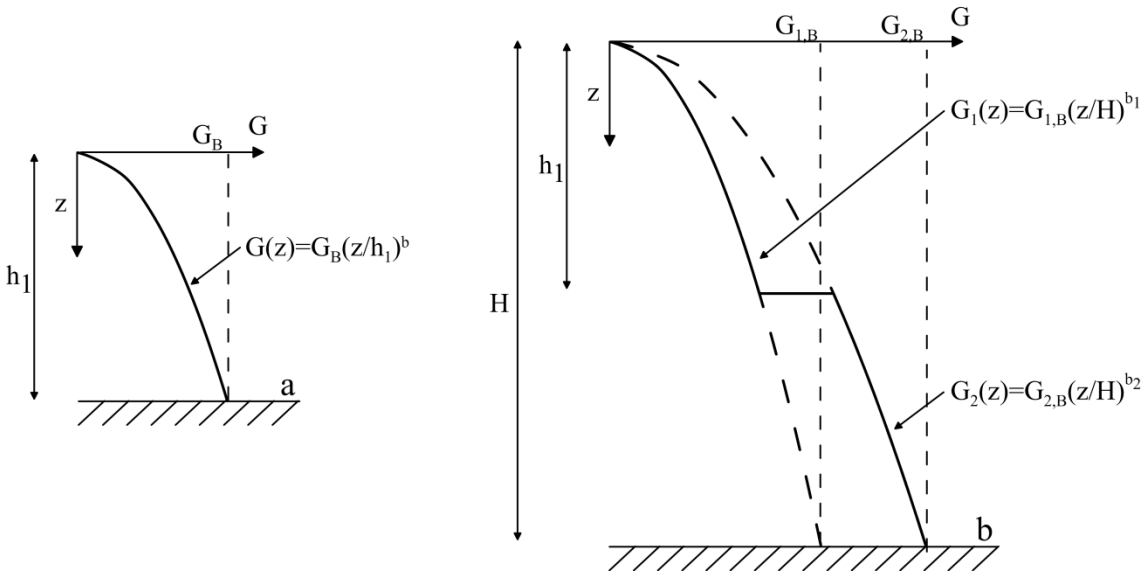

Figure 1. (a) Single inhomogeneous layer and (b) inhomogeneous two-layer deposit over a rigid base

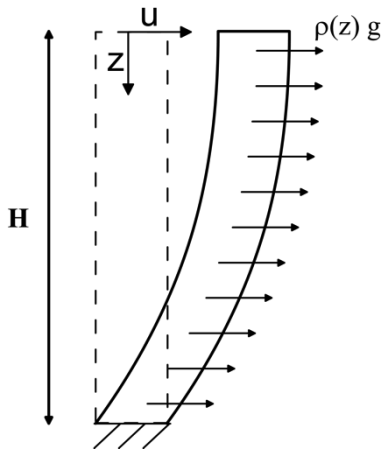

Figure 2. Soil model according to [13]

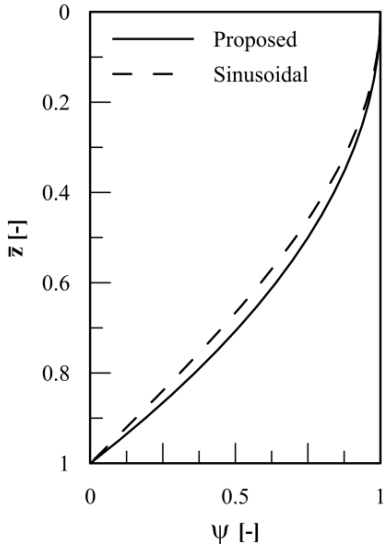

Figure 3. Shape functions for an homogeneous single layer

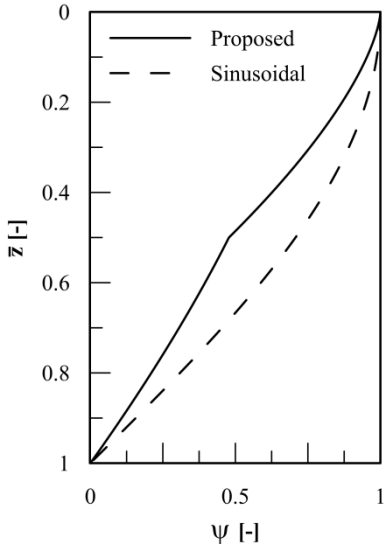

Figure 4. Shape functions for an inhomogeneous two-layer deposit

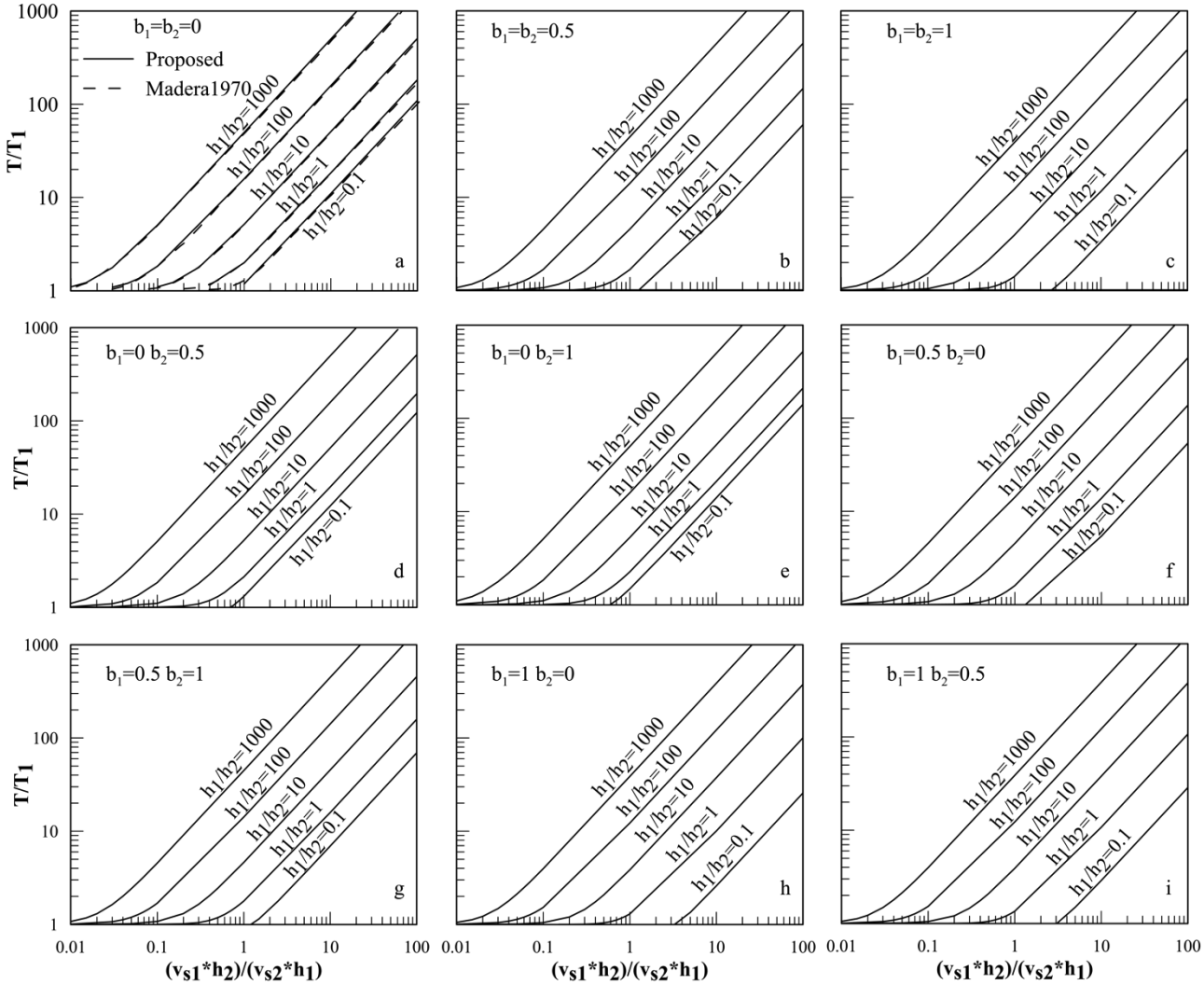

Figure 5. Graphical solutions for proposed method for over-consolidated clay over over-consolidated clay (a), sand over sand (b), normally-consolidated clay over normally-consolidated clay (c), over-consolidated clay over sand (d), over-consolidated clay over normally-consolidated clay (e), sand over over-consolidated clay (f), sand over normally-consolidated clay (g), normally-consolidated clay over over-consolidated clay (h) and normally-consolidated clay over sand (i)

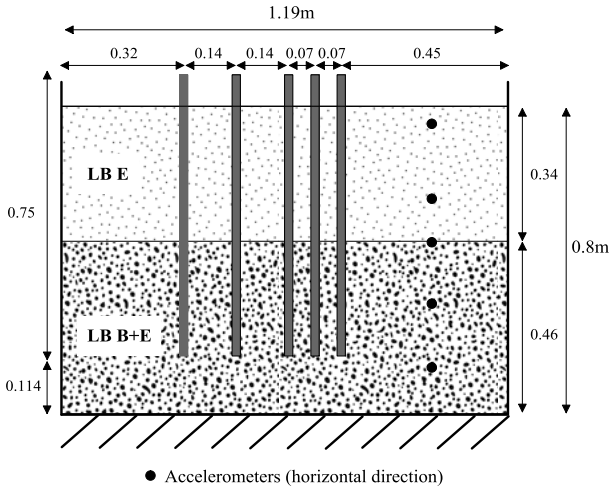

Figure 6. Model setup: subsoil and pile configuration

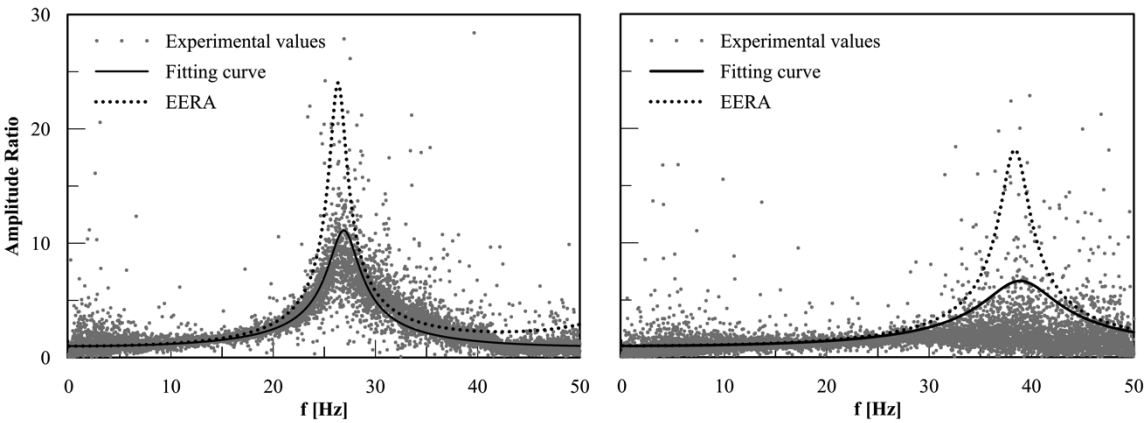

Figure 7. Transfer function of the whole system (left) and the top layer (right)

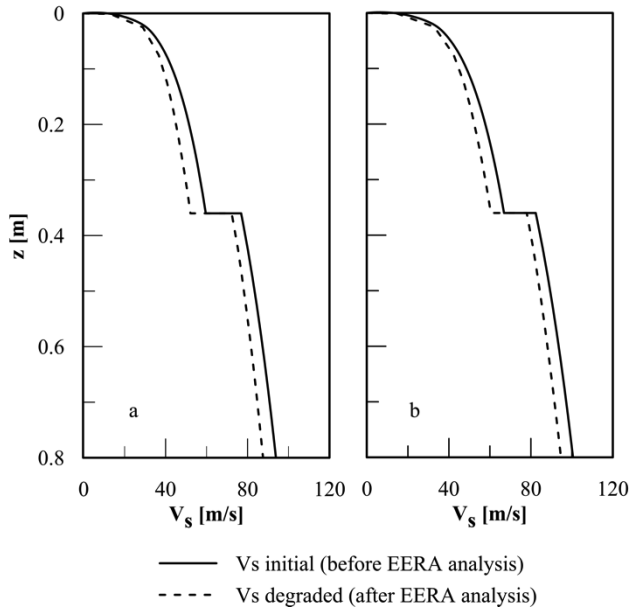

Figure 8. Initial and degraded shear wave velocity vs depth for the analytically computed profile (a) and the corrected one (b)

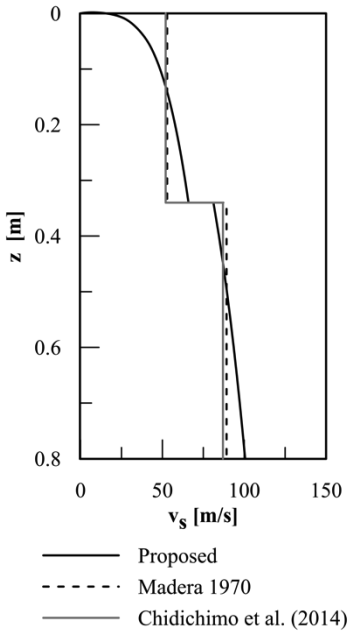

Figure 9. Initial shear wave profile for the analysed system

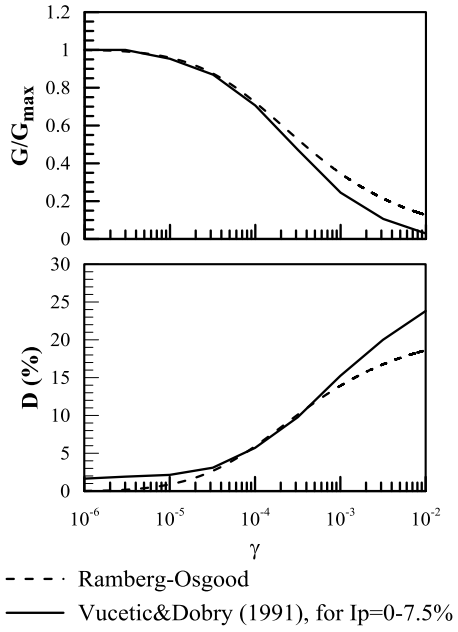

Figure 10. Comparison between Ramberg Osgood and Vucetic&Dobry curves for G/G_{max} and damping ratio vs strains

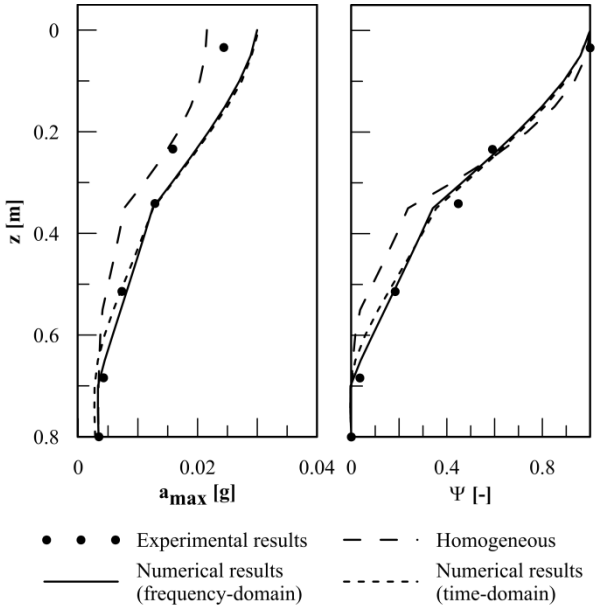

Figure 11. Envelopes of acceleration vs depth in free-field condition (left) and corresponding shape function (right) for *30* Hz sinedwell with input acceleration *0.003g*

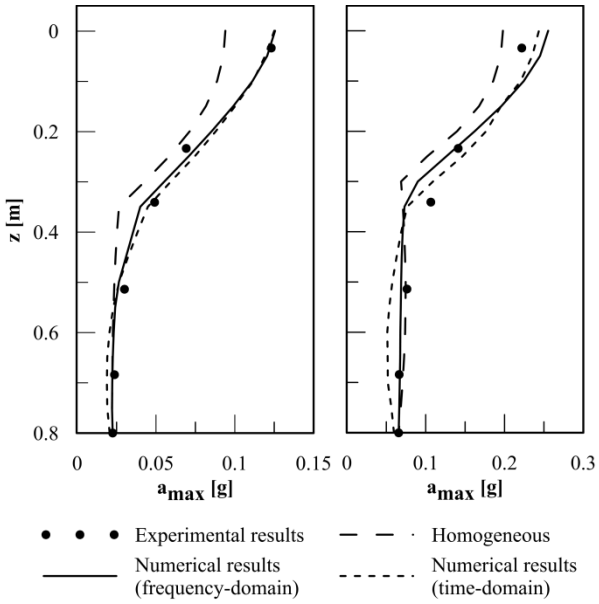

Figure 12. Envelopes of acceleration vs depth in free-field condition for *30* Hz sinedwell with input accelerations *0.02g* (left) and *0.06g* (right)

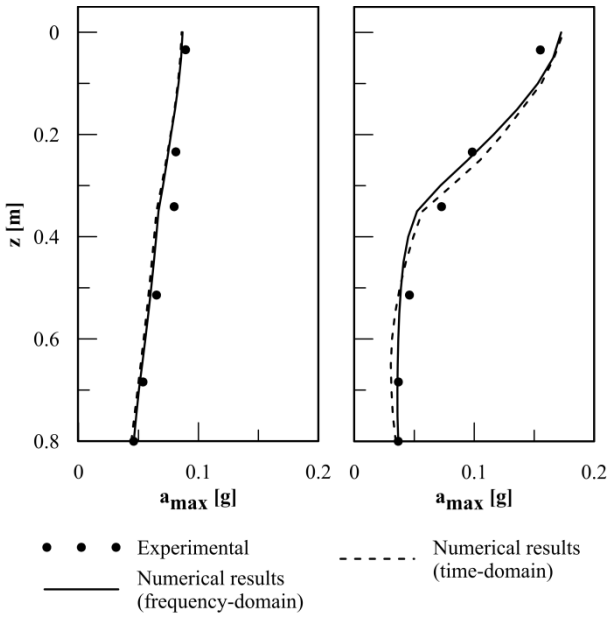

Figure 13. Envelopes of acceleration vs depth in free-field condition for sinedwell with input acceleration of 0.04g and frequency 15 Hz (left) and 30 Hz (right)